



## Progress towards realization of a laser IFE solid wall chamber

A.R. Raffray<sup>a,\*</sup>, J. Blanchard<sup>b</sup>, J. Latkowski<sup>c</sup>, F. Najmabadi<sup>d</sup>, T. Renk<sup>e</sup>,  
J. Sethian<sup>f</sup>, S. Sharafat<sup>g</sup>, L. Snead<sup>h</sup>,

the HAPL Team

<sup>a</sup> Mechanical and Aerospace Department and Center for Energy Research, 458 EBU-II,  
University of California, San Diego, 9500 Gilman Drive, La Jolla, CA 92093-0438, USA

<sup>b</sup> University of Wisconsin, Fusion Technology Institute, Madison, WI 53706, USA

<sup>c</sup> Lawrence Livermore National Laboratory, Livermore, CA 94550, USA

<sup>d</sup> Department of Electrical and Computer Engineering, Center for Energy Research,  
University of California, San Diego, La Jolla, CA 92093-0438, USA

<sup>e</sup> Sandia National Laboratories, Albuquerque, NM 87185, USA

<sup>f</sup> Naval Research Laboratory, Washington, DC, USA

<sup>g</sup> University of California Los Angeles, Los Angeles, CA, USA

<sup>h</sup> Oak Ridge National Laboratory, PO Box 2008, MS-6169, Oak Ridge, TN, USA

Received 16 April 2005; received in revised form 26 July 2005; accepted 26 July 2005

Available online 19 January 2006

### Abstract

The high average power laser (HAPL) program aims at developing laser inertial fusion energy (Laser IFE) based on lasers, direct drive targets and a solid wall chamber. The preferred first wall configuration is based on tungsten and ferritic steel as armor and structural materials, respectively. A key concern is the survival of the first wall under the X-ray and ion energy deposition from the fusion micro-explosion. The HAPL design and R&D effort in the chamber and material area is focused toward understanding and resolving the key armor survival issues. This includes modeling and experimental testing of the armor thermo-mechanical behavior in facilities utilizing ion, X-rays and laser sources to simulate IFE conditions. Helium management is addressed by conducting implantation experiments along with modeling of He behavior in tungsten. This paper summarizes the HAPL chamber activities. The first wall/armor configuration and design analysis are described, key chamber issues are discussed, and the R&D to address them is highlighted.

© 2005 Elsevier B.V. All rights reserved.

**Keywords:** Inertial fusion energy; Tungsten armor; Armor thermo-mechanical response; Ion implantation; He retention

### 1. Introduction

The high average power laser (HAPL) program is carrying out a coordinated and focused effort to develop

\* Corresponding author. Tel.: +1 858 534 9720; fax: +1 858 822 2120.

E-mail address: [raffray@fusion.ucsd.edu](mailto:raffray@fusion.ucsd.edu) (A.R. Raffray).

laser inertial fusion energy (Laser IFE) based on lasers, direct drive targets and a solid wall chamber [1]. IFE operation is cyclic (5–10 Hz) in nature and the wall is subjected repetitively to prompt energy deposition from the X-rays and ions produced by the fusion micro-explosion. As most of this energy is deposited within about 5–10  $\mu\text{m}$  of the surface, only a thin layer of the first wall is subject to high temperature cycles. Thus, the rest of the first wall and the blanket at the back essentially see steady state operation, akin to the MFE case. This was the basis for the selection of a configuration with a thin armor providing the threat accommodation function on a first wall providing the structural function. This approach also allows for the possible use of a number of compatible blanket designs that are being developed for MFE; thus, the IFE R&D resources can be more effectively directed to solving the IFE-specific armor/first wall issues, while maximum use can be made of all the information available from the MFE effort on blankets.

The preferred first wall configuration is based on tungsten and ferritic steel as armor and structural materials, respectively. A key issue is survival of the armor under the cyclic X-ray and ion threat spectra. Several possible mechanisms could affect the armor survival, including: failure of the armor due to ablation, melting, surface roughening and/or fatigue (due to cyclic thermal stresses); failure of the armor due to the accumulation of implanted helium; and failure of the armor/substrate bond due to fatigue. The HAPL design and R&D effort in the chamber and material area is focused toward understanding and resolving these major issues. The effort includes modeling and experimental testing of the armor thermo-mechanical behavior. Because the exact IFE ion and X-ray threat spectra on the armor cannot be duplicated at present, the experiments have to be performed in simulation facilities utilizing ion, X-ray and laser sources. Helium management is addressed by conducting implantation experiments along with modeling of He behavior in tungsten. The possibility of utilizing an engineered porous armor is also considered to help in enhancing the transport of implanted helium back to the chamber by minimizing the He diffusion length within the solid W; such a configuration might also help in accommodating thermal stresses.

This paper summarizes the HAPL chamber effort. The threats to the chamber wall are first characterized;

the first wall/armor configuration and design analysis are then described and example design windows for chamber operating parameters are shown; next, the key chamber issues are discussed and the modeling and experimental R&D effort to address them is highlighted; finally, conclusions are drawn, highlighting the key findings and summarizing the direction of future effort.

## 2. Threats

The analysis presented in this paper was based on the 154 MJ NRL direct-drive target shown in Fig. 1 [2,3]. The energy partitioning from this target, estimated from LASNEX calculations, is shown in Table 1 [4]. The major threats to the chamber wall are the ions which carry about 28% of the energy and, to a lesser extent (thermally), the photons which carry about 1% of the energy. Neutrons penetrate much deeper in the structure and blanket, and as such are a much lesser thermal threat to the chamber armor; however they would affect the ferritic steel structure lifetime. For

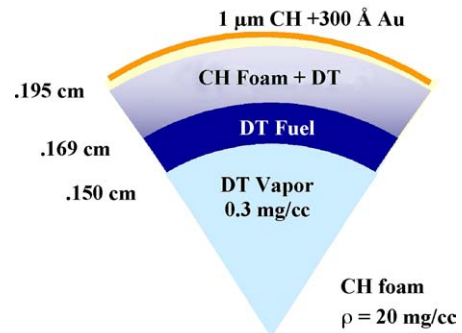


Fig. 1. Example direct drive target (NRL) to be coupled with a laser driver [2,3].

Table 1  
Energy partitioning for 154 MJ NRL direct-drive target [4]

	NRL direct-drive target (MJ)
X-rays	2.1 (1.4%)
Neutrons	109 (71%)
Gammas	0.009 (0.006%)
Burn product fast ions	19.5 (13%)
Debris ions kinetic energy	22.1 (14%)
Residual energy	1.29
Total	154

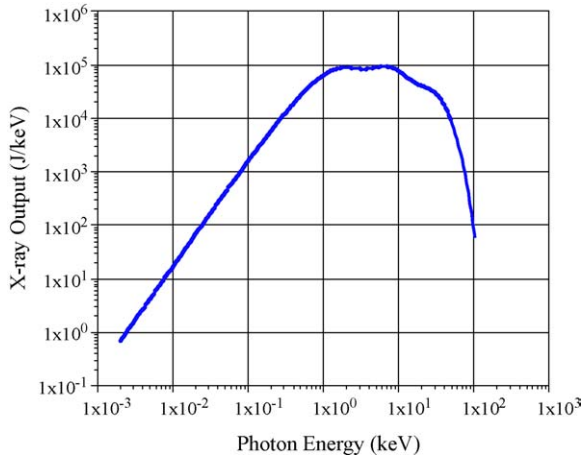


Fig. 2. Photon spectra from NRL 154 MJ direct-drive target and 458 MJ heavy ion beam indirect-drive target [4].

example, the 154 MJ target, produces about 109 MJ in neutrons, which, for an assumed chamber radius of 6.5 m and an assumed fusion power of 1800 MW (for a repetition rate of 11.7 Hz), corresponds to a time-averaged neutron wall load of about 2.4 MW/m<sup>2</sup>, or about 20 displacements per atom per full power year (dpa/fpy) in the first wall ferritic steel (with a corresponding first wall lifetime of about 5 fpy assuming a limit of ~100 dpa for ferritic steel). The neutron dpa in the tungsten armor is lower (~6 dpa/fpy) and any defects would probably be annealed out in the high-temperature region of the armor; however, the dpa due to the ion flux would be much higher and would not be annealed out if He occupies the induced vacancies; this needs to be considered as part of the He implantation and retention studies.

The photon spectrum is shown in Fig. 2 while the combined burn products (fast ions) and debris ions spectra for the 154 MJ direct-drive target are shown in Fig. 3. Higher yield direct-drive targets are also considered in the study but their energy partitioning and ion and photon spectra tend to be similar to those for the 154 MJ target; for the purpose of analysis, the relative energy partitioning and threat spectra from the 154 MJ target are used as representative of targets with different yields, with the energy levels being scaled accordingly. As a guide for evaluating the experimental simulations described in Section 5, the ion and X-ray fluences from the 154 MJ target on a chamber wall with

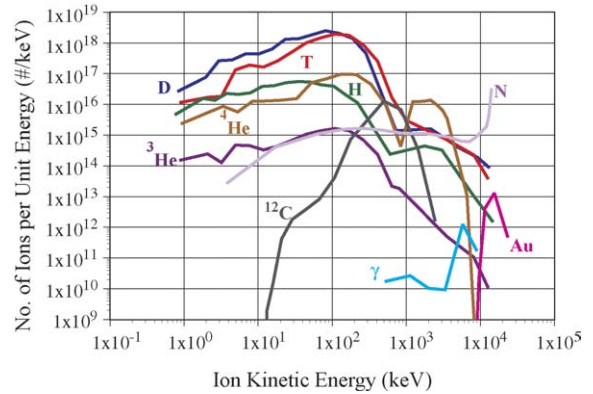


Fig. 3. Fast ion and debris ion spectra from NRL 154 MJ direct drive target [4].

a radius in the range 6.5–7.5 m are about 8–6 J/cm<sup>2</sup> and 0.4–0.3 J/cm<sup>2</sup>, respectively.

### 3. Armor/first wall configuration and thermal behavior

A refractory metal, such as tungsten, is an attractive armor candidate because of its high temperature capability and good thermal properties for accommodating the X-rays and ion energy deposition. In addition, tritium inventory (due to trapping in the bulk or to co-deposition as in the case of carbon) is not an issue. However, lifetime is a major concern, including: (i) the possibility of melting and whether this should be avoided; (ii) the thermo-mechanical response of the surface to the cyclic temperature gradients (which could lead to roughening or fracture); and (iii) the possibility of failure due to accumulation of implanted He ions. Representative properties of W are listed in Table 2 and used in the analysis presented in this paper.

Low activation ferritic (LAF) steel was selected as structural material. Oxide-dispersion strengthened (ODS) or nano-composited steel is considered as an alternate LAF structure as it would allow for a higher temperature of operation and possibly better bonding with tungsten. However, its data base is more limited and the practical aspects of its application such as forming and bonding will require greater R&D than the conventional LAF's.

Table 2  
Summary of typical tungsten material properties [7]

Thermo-physical properties	Tungsten
Density (kg/m <sup>3</sup> )	~19,350
Melting Point (K)	3683
Thermal conductivity (W/m K)	148 (500 K) 90 (3000 K)
Specific heat (J/kg K)	138 (500 K) 225 (3000 K)
Heat of fusion (kJ/kg)	192

The photon and ion energy deposition in the armor was calculated based on a 1D slab geometry for the spectra shown in Figs. 2 and 3 [5]. An attenuation calculation was used for the photon energy deposition based on data for the attenuation coefficient in the material as a function of the photon energy. The ion deposition calculation included both the electronic and nuclear stopping powers, which were obtained as a function of ion energy from SRIM [6]. The calculation procedure included the time of flight spreading of the photon and ion energy deposition. The photons travel much faster than the ions and would reach the chamber wall within about 20 ns over a time spread of less than 1 ns. The ions take longer to reach the chamber wall and would reach the wall at different times depending on their energy, thereby spreading the energy deposition over a longer time and lowering the peak heat generation in the wall. This is a key effect which needs to be included as an assumption of instantaneous energy deposition is overly conservative. Fig. 4 shows the power deposition as a function of penetration depth and time for W for the 154 MJ direct drive target spectra assuming a chamber radius of 6.5 m and no protective gas in the chamber.

The resulting armor thermal behavior is illustrated in Fig. 5, which shows the corresponding temperature history of a 1 mm W armor over a 2.5 mm ferritic steel substrate cooled by a 500 °C coolant. The photon energy deposition is very fast and creates the instantaneous temperature increase of about 1650 °C shown in the figure. The maximum W temperature following the energy deposition from the debris ions is about 2900 °C in this case. The figure shows that only a very thin armor region sees the high cyclic temperature rise, as the temperature peak falls to about 1500 °C at a depth of 10 μm and to only about 600 °C at a depth of 100 μm. This

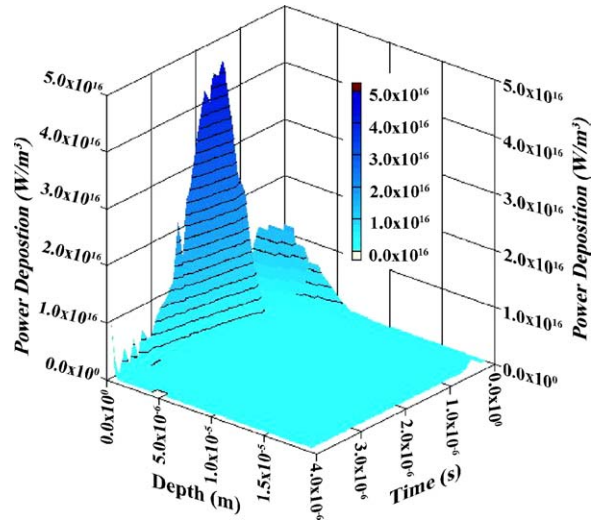


Fig. 4. Ion power deposition in tungsten armor as a function of time and penetration depth for the 154 MJ NRL direct-drive target in a chamber of radius 6.5 m with no protective gas.

was the basis for a first wall configuration with a thin armor layer to accommodate the high cyclic temperature rise over a structural wall which operates at quasi steady-state.

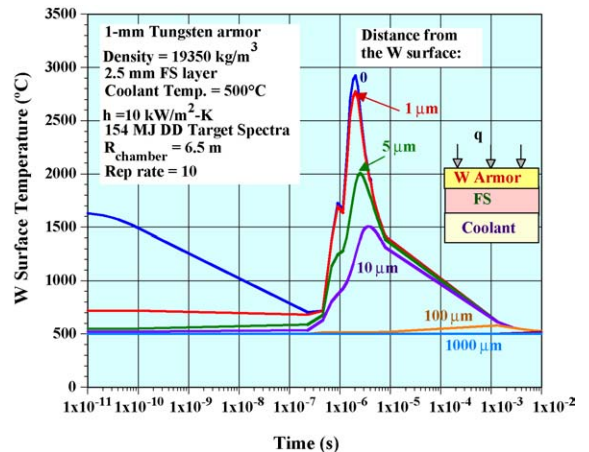


Fig. 5. Temperature history at different locations in a 1 mm W armor over a 2.5 mm ferritic steel substrate cooled by a 500 °C coolant based on the power deposition of Fig. 4 for the 154 MJ direct drive target spectra and assuming a chamber radius of 6.5 m and no protective gas in the chamber.

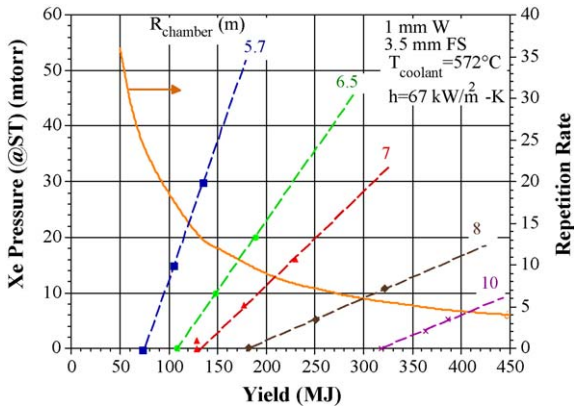


Fig. 6. Example integrated parametric study showing combinations of chamber gas density (shown as pressure at a standard temperature, ST = 300 K), yield and chamber size that would maintain the W armor temperature  $<2400^{\circ}\text{C}$  for a fusion power of 1800 MW and a coolant temperature of  $572^{\circ}\text{C}$ . The corresponding repetition rate for 1800 MW fusion is shown on the other vertical axis.

#### 4. Example parametric design window

It is not clear what is the most restrictive limit (temperature, thermal stress, cycling, He effects) to ensure a reasonable W armor lifetime. This will be determined from the results of the R&D effort described in the next section. To illustrate the impact of such a limit on the chamber design and operating parameters, the results from a parametric study assuming a maximum W temperature limit of  $2400^{\circ}\text{C}$  (based on some of the initial roughening results for tungsten, discussed in Section 5.1) are summarized in Fig. 6 [7]. These example results are based on a ferritic-steel first-wall thickness of 3.5 mm and a W armor thickness of 1 mm. The coolant temperature ( $572^{\circ}\text{C}$ ) and heat transfer coefficient ( $67 \text{ kW/m}^2 \text{ K}$ ) are compatible with an example self-cooled lithium blanket and 1800 MW fusion. The dashed lines show the combination of chamber protective Xe gas density (in terms of pressure at 300 K) and target yield that would limit the armor temperature to  $2400^{\circ}\text{C}$  for different chamber radii. From the figure, for this example, for a target yield of about 150 MJ, no protective gas would be required in a chamber of radius  $\sim 7.5 \text{ m}$ . For 1800 MW fusion, the repetition rate is rather high (11.7, shown by the solid line in the figure). For the same fusion power and a more modest repetition rate of  $\sim 5$ , the required yield is  $\sim 350 \text{ MJ}$ . In this case, a much larger chamber is required (of radius

10–11 m) for the case with no protective gas in the chamber. The presence of a protective gas would allow for a smaller chamber depending on the gas density (e.g.  $\sim 6.5 \text{ m}$  in radius for a Xe density of  $\sim 12 \text{ mtorr}$  at ST, and  $\sim 5.7 \text{ m}$  in radius for a Xe density of  $\sim 40 \text{ mtorr}$  at ST) but would adversely affect target injection, survival and placement and, possibly, laser propagation [5,8].

#### 5. HAPL armor/first wall R&D

A combination of experimental and modeling activities are being pursued as part of the HAPL R&D effort on chamber wall and armor to better understand the thermo-mechanical processes occurring in the armor and to help in deriving better limits on operating conditions of the armor/first-wall based on integrity and lifetime requirements. These include: simulation of the cyclic heat loads on the armor in ion beam, X-ray and laser facilities; studies of fatigue in the ferritic-steel/W bond; and studies of He implantation and retention. The range of testing facilities allows for the isolation of specific processes to help in understanding the governing mechanisms. For example, testing in an ion facility provides the combined effect of transient heating and ion bombardment whereas testing in a laser facility only provides the effect of transient heating. Comparison of the results from these two facilities will help identify whether the lifetime limiting processes in the armor is only temperature (and temperature-gradient) driven or whether ion bombardment also plays a major role.

##### 5.1. Ion facility

Ion exposures are conducted at the repetitive high energy pulse power (RHEPP-1) facility at Sandia National Laboratories (SNL). RHEPP delivers an ion beam with energy of up to 800 keV for singly-charged He ions, and up to 1.6 MeV for doubly-charged N ions (about half the total N beam), with a pulse-width of 100–300 ns. The energy is within the range of energy expected from IFE (see Fig. 3) but the pulse-width is shorter than the few  $\mu\text{s}$  expected for IFE (see Fig. 4). Studies have focused on determining the roughening thresholds for different armor sample materials [9,10]. The formation of surface relief is of concern for two reasons. The resulting surface morphology may prove

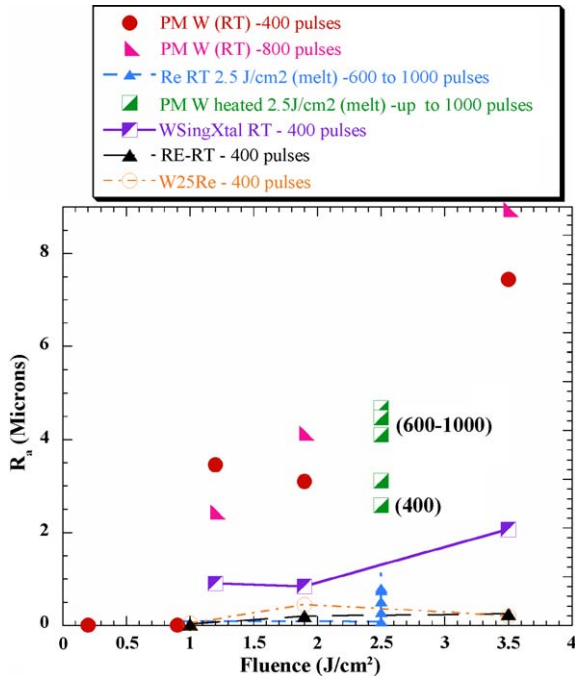


Fig. 7. Surface roughness as a function of fluence for different samples tested in the RHEPP facility.

to be mechanically unstable, i.e. may result in material loss due to exfoliation or similar mechanism. In addition, surface structures such as microcracks may act as initiation sites for fatigue cracks which could then propagate below the surface. The preliminary findings indicated that roughening increases rather linearly with the number of pulses at a given ion fluence. It also increases with the fluence per pulse. Surface relief was observed after about 200 pulses, and surface profilometry measurements suggest that, in the case of tungsten, the build-up of relief may saturate. This would have to be verified by testing over more prototypic number of pulses (more amenable to testing in a rapid cyclic heat load facility such as under a laser beam). A summary of exposure results is given in Fig. 7, which shows surface roughening behavior as a function of average N beam fluence for the following materials: powder metallurgy W (PM W) at both room temperature (RT) and 520 °C, single-crystal W at RT, and W25Re and Re at RT. Surface roughening is measured by 1D profilometry (DekTak). The 520 °C heated temperature more nearly simulates reactor conditions, and also raises the

bulk temperature above the brittle–ductile transition temperature (DBTT) for tungsten. W25Re is studied because the added Re increases the ductility of the alloy. Pure Re is of interest not as a candidate armor material, but because Re lacks a DBTT, and so work-hardens immediately upon mechanical processing. Thus, it may be expected to exhibit the most significant morphology changes due to ion exposure.

Care should be taken in interpreting results from cyclic testing in RHEPP-1 since the energy deposition from cycle to cycle might vary by a significant factor, up to about  $\pm 50\%$  [10]. For example, a sample under an average fluence which should not cause melting could have actually operated at above the melting point for a fraction of the cycles. Given this caveat, some general observations can be made from the results shown in Fig. 7:

- The roughening trends appear to be independent of the predicted surface melting temperature for W ( $\sim 3410^\circ\text{C}$  corresponding to a fluence of  $\sim 2\text{--}2.5\text{ J/cm}^2$ ). This is probably because even at  $3.5\text{ J/cm}^2$ , the total melt duration is predicted to be less than 150 ns, and the inertial response of the initially solid metal can be expected to be negligible on this time-scale.
- The roughening threshold for tungsten fabricated from PM W seems to be about  $1\text{ J/cm}^2$  at room temperature. Below this value, the PM W surface (RT) appears unaffected by ion exposure, as indicated by SEM observation at up to 15,000 magnification. In particular, no micro-cracking of the surface is evident. Above the threshold, surface roughening seems to increase rapidly with fluence, and, to a lesser extent, with the number of pulses.
- Single crystal W shows less roughening than powder-met W, and possibly a higher threshold also.
- Heating the PM W reduces the roughening and possibly increases the threshold but as the PM W data points at  $2.5\text{ J/cm}^2$  show, with additional pulses (up to 1000), the roughness reaches the level of the PM W RT trend line.
- Rhenium (Re) shows much better resistance to roughening than W; and so does the alloy of 25% Re–75% W. Even at 1000 pulses for Re at  $2.5\text{ J/cm}^2$ , the roughness is less than  $1\text{ }\mu\text{m}$ . However, the surfaces of both Re and 25% Re–75% W are observed to undergo micro-cracking at levels of fluence below

that for which PM W shows no beam effect. The lower limit of this microcracking is currently not known, but seems to be  $<0.8 \text{ J/cm}^2$  in either case.

Note that one has also to be very careful when extrapolating these initial results to prototypic conditions (aside from the experimental uncertainty). For example, the energy level of the ion beam would result in the heated sample melting at about a fluence slightly over  $2 \text{ J/cm}^2$ . The W armor in an IFE reactor under the energy deposition from the ion spectra shown in Fig. 3 would require more than four times this fluence to reach the melting point. Thus, these preliminary results are useful in identifying some general trends but more controlled experimental results (in conjunction with testing in the other facilities) and more detailed modeling are required to help better understand the thermo-mechanical response of the armor and guide the final choice of armor/first-wall configuration and operating limits. Under this understanding, a rough initial W armor temperature limit of  $2400 \text{ }^\circ\text{C}$  (corresponding roughly to a fluence of  $\sim 1.2 \text{ J/cm}^2$  in RHEPP-1 for a heated sample) was assumed to help in the armor design calculations in integration with the other IFE chamber interfacing components. This is a working number to be updated as more data become available.

## 5.2. X-ray facilities

The XAPPER facility of Lawrence Livermore National Laboratory (LLNL) is used to perform pulsed testing of armor samples subject to X-rays. XAPPER is based upon an extreme ultraviolet (EUV) X-ray source designed and built by PLEX LLC using a plasma pinch as source [11]. An ellipsoidal focusing optic is used to increase the per-shot X-ray fluence to  $\sim 1 \text{ J/cm}^2$  over a spot size of  $\sim 1 \text{ mm}$ . The X-ray spectra show energy around  $100 \text{ eV}$ . This is about one order of magnitude lower than the typical IFE X-ray energy shown in Fig. 2, but the attainable fluence for the given spectra is sufficient to reproduce the peak temperature of the W armor under the IFE spectra (with melt occurring at a fluence of about  $1\text{--}1.2 \text{ J/cm}^2$ ). However, the time deposition of the energy is short, of the order  $\sim 0.01 \text{ } \mu\text{s}$  compared to the  $\sim 1 \text{ } \mu\text{s}$  in the IFE case (governed by the time of flight of ions). Samples can be irradiated with up to  $10^5\text{--}10^6$  pulses (the latter requiring about 28 h of continuous testing).

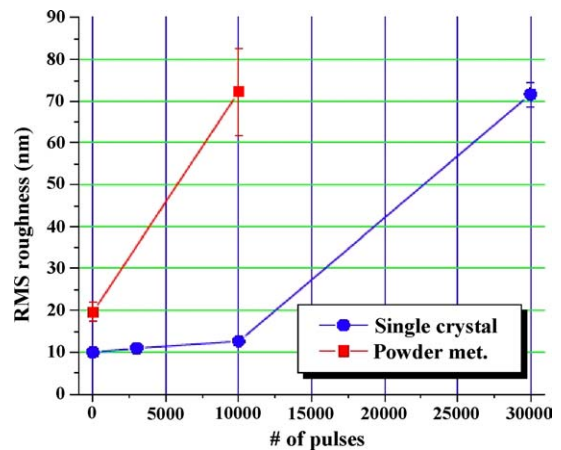


Fig. 8. Surface roughness in powder-metallurgy and single crystal tungsten as a function of number of pulses from tests in the XAPPER facility.

The initial results from X-ray irradiation of a W sample are summarized in Fig. 8, which shows roughening in PM W and single-crystal W as a function of the number of cycles for a per-shot fluence of about  $1 \text{ J/cm}^2$ . The results suggest that there may be a threshold above which roughening occurs with the threshold being somewhat higher for the single crystal case. Further experiments are needed to understand better whether the roughening increases linearly with number of pulses and also whether it saturates after a number of cycles. One major improvement would be to be able to measure the surface temperature during the cycle to provide a better understanding of the behavior of the material and of how well it can simulate the actual IFE case. An optical thermometer developed and built at the University of California, San Diego (UCSD) is being installed for this purpose.

Single shot X-ray exposure is also performed in the Z-machine of SNL [10], which can provide up to  $10 \text{ keV}$  X-rays. Tungsten samples (single crystal, powder metallurgy and chemical vapor deposition) were exposed to various fluences in the Z-machine (with some samples preheated to  $600 \text{ }^\circ\text{C}$ ). The results showed no melting below a fluence of  $1.3 \text{ J/cm}^2$ . Another set of samples were heated to  $600 \text{ }^\circ\text{C}$  and exposed to fluences of  $0.27$  and  $0.9 \text{ J/cm}^2$ . The surfaces were examined with two-dimensional VEECO profilometry, and were carefully analyzed compositionally to separate the effects of surface roughening from the debris field

on each sample. The surface appearance of the polycrystalline samples, i.e. the PMW and CVD W, is different from the single-crystal W, with an indicated roughening threshold between 0.3 and 0.9 J/cm<sup>2</sup>. The Single-crystal sample showed no evidence of roughening at 0.9 J/cm<sup>2</sup>. Therefore, the roughening threshold for single-crystal W appears higher for Z X-ray exposure than for the other W polycrystalline samples.

### 5.3. Laser facility

Laser testing of armor samples is performed at the Dragonfire facility at UCSD. Modeling has shown that the IFE W armor surface temperature history and to some extent the spatial temperature profile can be duplicated by adjusting the laser pulse. The samples are heated using a YAG laser with a rep rate of 10 Hz. The high rep-rate of the laser allows testing to 10<sup>5</sup>–10<sup>6</sup> cycles [12]. A key effort in setting up this experiment was the development of a high-speed optical thermometer to measure the real-time temperature of sample surface with ns resolution. Additional diagnostics, such as QMS and RGA to measure and characterize per-shot ejecta and constituents are installed. A high-temperature sample holder is included to allow for testing with the armor sample at prototypical “equilibrium” temperature.

From the initial results on powder metallurgy W samples, it appears that the samples evolve at two different time scales, where defect planes appear at low shot counts (~10<sup>3</sup> shots) and individual “nuggets” (with higher roughness) appear over the high shot counts (~10<sup>5</sup> shots). It was also observed that the samples at the higher base temperature show less damage. For example, for 1000 shots and a temperature increase of about 2500 °C, a sample at a 500 °C base temperature shows almost no damage whereas a room temperature sample shows clear damage. This is also seen with higher shot counts but the difference between the two samples is less marked. Future effort will help to understand better these preliminary observations and to observe the effect of testing with higher shot counts on sample roughening. A particularly interesting comparison would be to test two identical samples at the same base temperature and up to the same peak temperature in the ion facility (RHEPP), in the X-ray facility (XAPPER) and in the laser facility (Dragonfire) over the same number of cycles (~10<sup>3</sup>) to determine under

these conditions the individual effect of temperature, ion implantation and any X-ray damage.

### 5.4. Infrared facility

The infrared processing facility at the Oak Ridge National Laboratory (ORNL) is used for fatigue testing the W armor/ferritic steel (F82H) substrate bond [13]. Two bonding processes are considered: diffusion-bonded tungsten foil (~0.1 mm) to ferritic steel and plasma-sprayed tungsten transition coatings which allows for a graded transition from ferritic steel to tungsten. Means of achieving higher W thicknesses (~1 mm) are also being investigated. Post-spray treatments to provide annealing and stress relief are also included. Thermal fatigue testing has been carried out at 10 Hz, 10 ms pulses width, and ~20 MW/m<sup>2</sup> (chosen to simulate IFE tungsten/steel interfacial stress.) Materials include 0.1 mm thick W coated LAF samples of 25 mm × 25 mm × 5 mm. The base temperature of the interface was 600 °C. The lack of spalling and overall integrity of the bond following thousands of pulsed indicate good adhesion. The long-term microstructural stability of the interface using diffusion couples and additional thermal fatigue testing is underway.

### 5.5. Modeling

Pre- and post-experimental analyses are required to help plan and understand results from the experimental facilities mentioned above. Models such as those used to generate the energy deposition and temperature profiles shown in Figs. 4 and 5 are very useful in this respect. In addition thermo-mechanical models are required to better understand the thermal stress behavior as well as any crack initiation and growth. For example, results from ANSYS finite element analyses can provide the stress intensity for a given crack size which may be compared with the material fracture toughness and crack growth rates to determine if a crack would propagate to the substrate. The stress intensity factor changes with crack depth because of variations in the tungsten stress through the material depth as well as modifications of the crack geometry. Models were generated with crack depths ranging from 15 to 150 μm, and the stress intensities were calculated. The results are illustrated in Fig. 9 [14]. The stress intensity falls from over 10 MPa m<sup>1/2</sup> for the 15 μm

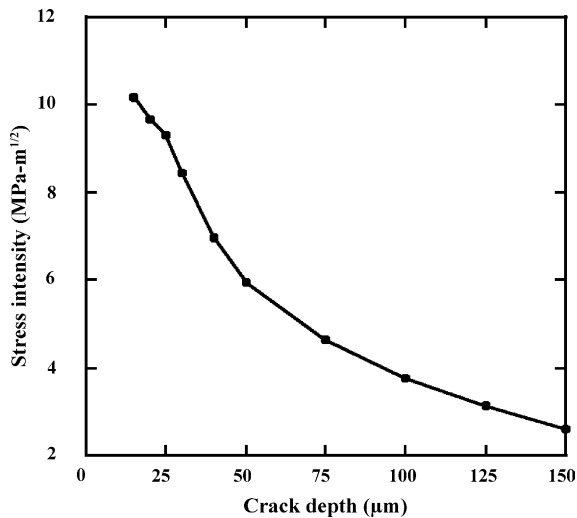


Fig. 9. Variation of fracture stress intensity with crack depth in the tungsten armor. Results after a single pulse with 1 mm crack spacing.

crack to  $2.6 \text{ MPa m}^{1/2}$  for the  $150 \text{ μm}$  crack. The reduction in the stress intensity with crack depth indicates that cracks that initiate at the surface may stop before reaching the armor/steel interface. Further analysis of the effect of crack spacing (assumed as 1 mm for the above results) indicates that the stress intensity drops to zero for deeper cracks with smaller spacings and a possible scenario would be for a number of closely spaced cracks to initiate at the armor surface where the stress intensities are highest, and the propagation of many or all of these cracks might stop less than  $100 \text{ μm}$  into the surface. There is limited fracture mechanics data for thin tungsten films, especially when subjected to these extreme temperature cycles, so prediction of fracture behavior is difficult. Data on crack growth rates is needed to make conclusive predictions of the ultimate fate of the cracks.

Stresses and fatigue in the ferritic steel substrate are also of concern since while one might imagine tolerating surface cracks in the tungsten, it is difficult to imagine tolerating cracks in the steel. Hence, the primary concern in the steel is high cycle fatigue. Data for F82H at several thousand cycles indicate that stress amplitudes of over 400 MPa will yield lifetimes of well over 100,000 cycles. There are no data beyond this cycle level to determine the stresses needed to ensure  $10^8$  cycles as needed for HAPL. However, data from other steels (such as 12Cr–2W ferritic steel) indicate

a lifetime  $>10^8$  cycles at stress amplitudes  $>300 \text{ MPa}$  at  $400 \text{ °C}$ , which is a level of over 0.5 times the yield stress. Hence, there is a significant margin in the steel stress levels since the tensile stresses in a typical HAPL cycle are not as high as the compressive stresses, whereas the tests are done with a mean stress of 0 [14].

### 5.6. He retention studies

These studies are focused on investigating the helium retention and surface blistering characteristics of tungsten with regard to helium dose and temperature (as well as the effect of deuterons). Ultimately, the goal is to determine if helium retention can be mitigated by the pulsed nature of the helium implantation in combination with the high temperature thermal spikes within the IFE reactor (e.g., see Fig. 5). The experimental activities are performed through a collaboration between the University of North Carolina and ORNL (high base temperature,  $\sim 850 \text{ °C}$ , high energy,  $\sim 1.3 \text{ MeV}$ , pulsed implantation and anneals at  $2000 \text{ °C}$  over  $\sim 1000$  cycles to fluences of  $\sim 10^{20} \text{ He/m}^2$ ) [15] and, separately, by the University of Wisconsin in Madison (high temperature,  $\sim 800 \text{ °C}$  or more, modest energy,  $\sim 10\text{--}100 \text{ keV}$ , pulsed implantation to fluences of  $\sim 10^{22} \text{ He/m}^2$ ) [16].

Initial experimental results indicated that the first wall of an IFE fusion reactor may suffer from significant damage due to helium trapping and bubble formation under the high fluences of helium ions and intense temperatures. However, the data also suggest that certain conditions may mitigate this effect. Less trapping of helium was observed in single crystal material under certain conditions when compared to polycrystalline tungsten, as illustrated in Fig. 10 from the He implantation and anneal study [13]. More importantly, the results indicate that He retention decreases drastically when a given helium dose is spread over an increasing number of pulses, each one followed by W annealing to  $2000 \text{ °C}$ , to the extent that there would be no He retention below a certain He dose per pulse. For example, from Fig. 10, for single crystal tungsten, this threshold would be of the order of  $10^{16} \text{ ions/m}^2$  per shot. For the 154 MJ spectra shown in Fig. 3, this threshold is still too high as the He dose per shot in a chamber of radius  $\sim 7.5 \text{ m}$  is  $\sim 7.5 \times 10^{16} \text{ ions/m}^2$ . However, for the IFE case the maximum W armor surface temperature would be higher,  $\sim 2400 \text{ °C}$ , which

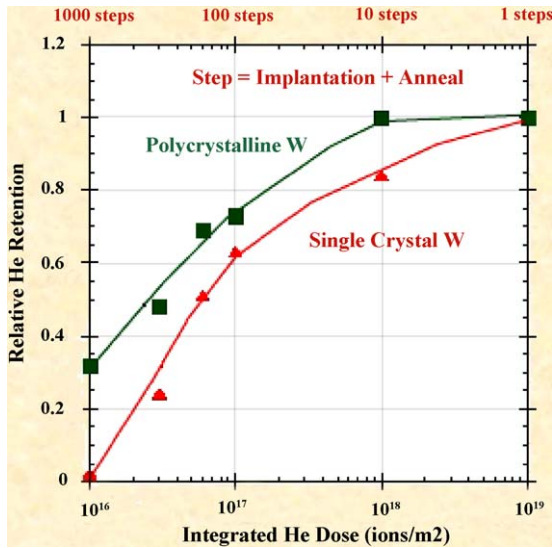


Fig. 10. Relative He retention in polycrystalline and single crystal W samples as a function of integrated He dose for different number of pulses [13].

would significantly increase the helium mobility and, thus, should also significantly increase the per-shot threshold at which helium begins to accumulate. Currently, research is underway to better understand the kinetics of helium at these higher temperatures. Thus, the trends are promising but more R&D is required to make a better assessment of He behavior in the IFE case. This R&D includes both experimental work and modeling work currently performed at the University of California, Los Angeles with the HEROS code [17].

HEROS is a newly developed helium bubble evolution code based on kinetic rate theory to study a wide range of helium implantation conditions including the atom displacement effect of the incident ions. Whereas the high operating temperature of the armor would anneal out most defects due to neutron-induced dpa, the presence of He ions in the vacancies created by the ion-induced dpa effect prevents this annealing process. The code is unique in that for the first time spatially dependent phenomena including loss of point defects, interstitial helium, vacancy-helium clusters, and bubbles lost to free surfaces are included. The code input estimates helium bubble density and size distributions based on prototypical helium implantation conditions. Furthermore, time and spatially dependent temperature distributions are used to calculate helium bubble

behavior in the armor during the implantation pulse. First results have shown that the helium bubble densities rise during the implantation period of an HAPL IFE pulse, but drastically drop during the ensuing high temperature spike (with a temperature rise of  $\sim 2200^\circ\text{C}$ ) [17]. Calibration of the HEROS code with experimental results is continuing.

The possibility of utilizing engineered material to enhance the release of implanted helium is also being investigated. The goal is to minimize the migration distance of helium in the tungsten structure, which, coupled with the high temperature of operation, could help implanted helium migrate out of the structure. Such a fine structure could be part of a configuration with interconnected porosity, which would provide the helium a subsequent path of least resistance to the chamber. The porous structure could also help in accommodating local thermal stresses and minimize possible lifetime-limiting mechanisms such as micro-crack formation and propagation and/or roughening. Two possible engineered tungsten structures have been proposed as armor candidates: a high porosity foam proposed by Ultramet which is described in detail in Ref. [18]; and a nano-sized homogeneous porous region proposed by PPI whose initial thermal performance analysis is summarized in Ref. [7]. The latter material in particular is in its early development phase and more R&D is required to have a better assessment of the suitability of such engineered material as IFE chamber armor.

## 6. Conclusions

The HAPL program is aimed at developing Laser IFE based on a laser driver, direct drive targets and a solid wall chamber. The preferred first wall configuration is based on a thin W armor providing the high energy accommodation function bonded to a ferritic steel substrate providing the structural function and interfacing with the coolant and blanket (which operate under quasi steady-state conditions).

A key concern is the survival of the first wall under the X-ray and ion energy deposition from the fusion micro-explosion. The HAPL design and R&D effort in the chamber and material area is focused toward understanding and resolving the key issues that could affect the armor survival. The effort includes experimental

and modeling activities to better understand the armor thermo-mechanical behavior under the pulsed energy deposition and the behavior of the implanted He in the W armor. Encouraging results have been obtained from initial testing in a range of facilities. It is not yet clear how to extrapolate the results to the IFE case as fully integrated conditions (such as energy deposition profiles in time and space) have not been reproduced; thus, the results have to be interpreted carefully and the ongoing R&D effort will help to shed more light on these armor survival issues. However, a number of general observations on the armor behavior and possible trends can be made:

- Surface roughening of the armor has been observed in all facilities (ion beam, X-ray and laser). It seems that a possible threshold exists for armor roughening based on a combination of temperature, fluence and energy deposition profiles. This threshold has yet to be fully characterized for IFE conditions and the individual roles played by the thermal conditions and the ion implantation still need to be determined. Also, it is not clear how roughening increases with number of pulses and whether it saturates after a number of cycles or whether it leads to mass loss.
- From the RHEPP-1 ion beam facility test results, it appears that: single crystal W shows less roughening than powder-met W; Re shows much better resistance to roughening than W; and so does the alloy of 25% Re–75% W. Also, armor samples at a higher base temperature tend to show less damage (as compared to room temperature samples), but the relative differences seem to decrease with increasing number of cycles (also seen in the preliminary results from tests performed in the Dragonfire laser facility). However, there is a substantial variation in shot to shot ion beam fluence on the samples and these observations need to be further verified.
- Initial results from fatigue testing of the W/ferritic-steel bond indicate good adhesion of the coating (no spalling). Long term thermal stability studies are under way.
- Modeling studies indicate the possibility of cracks initiating at the armor surface where the stress intensities are highest, but propagating to less than 100  $\mu\text{m}$  from the surface. Castellating the armor would help accommodate the stresses and reduce crack propagation concerns. Data on crack growth rates is needed to make conclusive predictions of the ultimate fate of the cracks.
- There seems to be a significant margin in the steel stress levels to accommodate the cyclic stress without crack formation in the ferritic steel substrate.
- Helium trapping in W is a key concern as it can lead to surface damage and armor failure. Initial results indicate that there might be a He flux per shot threshold below which the implanted He will be released during the temperature excursion. This threshold is higher for single crystal W as compared to powder met W. Future modeling and experimental effort should help to better understand this effect under IFE prototypical conditions.

In conclusion, although some major issues still need to be resolved, the analyses show encouraging results for the possibility of utilizing a W-armored chamber in combination with a laser-driven direct-drive target. The major chamber armor and wall issues have been identified and are being addressed through a combination of modeling and experimental R&D. Future effort will help to understand better some of the observations and trends from the initial rounds of testing.

### Acknowledgement

This work was supported in part by a grant from the Naval Research Laboratory, award No. N00173-01-1-G906.

### References

- [1] J.D. Sethian, A.R. Raffray, J. Latkowski, J.P. Blanchard, L. Snead, T.J. Renk, S. Sharafat, Considerations for the chamber first wall material in a laser fusion power plant, *J. Nucl. Mater.* 347 (3) (2005) 161–177.
- [2] S.E. Bodner, G. Colombant, A.J. Schmitt, M. Klapisch, High-gain direct-drive target design for laser fusion, *Phys. Plasmas* 7 (6) (2000) 2298–2301.
- [3] D.T. Goodin, N.B. Alexander, C.R. Gibson, A. Nobile, R.W. Petzoldt, N.P. Siegel, L. Thomson, Developing target injection and tracking for inertial fusion energy power plants, *Nuclear Fusion* 41 (2001) 527–536.
- [4] Available at <http://aries.ucsd.edu/ARIES/WDOCS/ARIES-IFE/SPECTRA/>.
- [5] A.R. Raffray, et al., the ARIES Team, Dry wall survival under IFE conditions, *Fusion Sci. Technol.* 46 (2004) 417–437.
- [6] Available at <http://www.srim.org/>.

- [7] A.R. Raffray, the HAPL Team, Chamber threats, design limits and design windows, *J. Nucl. Mater.* 347 (3) (2005) 178–191.
- [8] F. Najmabadi, A.R. Raffray, et al., The ARIES-IFE Team, Design windows for dry wall and thin-liquid protected IFE chambers, *Fusion Sci. Technol.* 46 (2004) 401–416.
- [9] T. Renk, P.P. Provencio, T.J. Tanaka, C.L. Olson, R.R. Peterson, J.E. Stolp, D.G. Schroen, T.R. Knowles, Chamber wall materials response to pulsed ions at power-plant level fluences, *J. Nucl. Mater.* 347 (3) (2005) 266–288.
- [10] T. Renk, et al., Laser inertial fusion dry-wall materials exposure to X-rays and ions, in: presented at the US/Japan Workshop on Laser IFE, General Atomics, San Diego, CA March 2005, available at: <http://aries.ucsd.edu/LIB/MEETINGS/0503-USJ-LIFE/program.shtml>.
- [11] J.F. Latkowski, R.P. Abbott, R.C. Schmitt, B.K. Bell, Effect of multi-shot X-ray exposures in IFE armor materials, *J. Nucl. Mater.* 347 (3) (2005) 255–265.
- [12] F. Najmabadi, IFE chambers: modeling and experiments at UCSD, presented at the US/Japan Workshop on Laser IFE, General Atomics, San Diego, CA (March 2005), available at: <http://aries.ucsd.edu/LIB/MEETINGS/0503-USJ-LIFE/program.shtml>.
- [13] L. Snead, et al., Refractory armored first wall development, in: presented at the US/Japan Workshop on Laser IFE, General Atomics, San Diego, CA, March 2005, available at: <http://aries.ucsd.edu/LIB/MEETINGS/0503-USJ-LIFE/program.shtml>.
- [14] J.P. Blanchard, C.J. Martin, Thermomechanical effects in a laser IFE first wall, *J. Nucl. Mater.* 347 (3) (2005) 192–206.
- [15] S.B. Gilliam, S.M. Gidcumb, N.R. Parikh, D.G. Forsythe, B.K. Patnaik, J.D. Hunn, L.L. Snead, G.P. Lamaze, Retention and surface blistering of helium irradiated tungsten as a first wall material, *J. Nucl. Mater.* 347 (3) (2005) 289–297.
- [16] B.B. Cipiti, G.L. Kulcinski, Helium and deuterium implantation in tungsten at elevated temperatures, *J. Nucl. Mater.* 347 (3) (2005) 298–306.
- [17] S. Sharafat, N. Ghoniem, Comparison of a microstructure evolution model with experiments on irradiated vanadium, *J. Nuclear Mater.* 283–287 (2) (2000) 789–793.
- [18] S. Sharafat, N.M. Ghoniem, M. Anderson, B. Williams, J. Blanchard, L. Snead, The HAPL Team, Micro-engineered first wall tungsten armor for high average power laser fusion energy systems, *J. Nucl. Mater.* 347 (3) (2005) 217–243.